NeuroImage xxx (2011) xxx–xxx

Contents lists available at SciVerse ScienceDirect

NeuroImage

journal homepage: www.elsevier.com/locate/ynimg

Magnetic resonance imaging of the Amine–Proton EXchange (APEX) dependent contrast

Tao Jin *, Ping Wang, Xiaopeng Zong, Seong-Gi Kim

Neuroimaging Laboratory, Department of Radiology, University of Pittsburgh, Pittsburgh, PA, 15203, USA

ARTICLE INFO

Article history:
Received 31 May 2011
Revised 3 August 2011
Accepted 9 August 2011
Available online xxxx

Keywords:
Amine–water proton exchange
Spin-locking MRI
Amino acids
Proteins
Ischemia
Amide–proton transfer
Chemical exchange saturation transfer

ABSTRACT

Chemical exchange between water and labile protons from amino-acids, proteins and other molecules can be exploited to provide tissue contrast with magnetic resonance imaging (MRI) techniques. Using an off-resonance Spin-Locking (SL) scheme for signal preparation is advantageous because the image contrast can be tuned to specific exchange rates by adjusting SL pulse parameters. While the amide–proton transfer (APT) contrast is obtained optimally with steady-state preparation, using a low power and long irradiation pulse, image contrast from the faster amine–water proton exchange (APEX) is optimized in the transient state with a higher power and a shorter SL pulse. Our phantom experiments show that the APEX contrast is sensitive to protein and amino acid concentration, as well as pH. In vivo 9.4-T SL MRI data of rat brains with irradiation parameters optimized to slow exchange rates have a sharp peak at 3.5 ppm and also broad peak at −2 to −5 ppm, inducing negative contrast in APT-weighted images, while the APEX image has large positive signal resulting from a weighted summation of many different amine-groups. Brain ischemia induced by cardiac arrest decreases pure APT signal from ~1.7% to ~0%, and increases the APEX signal from ~8% to ~16%. In the middle cerebral artery occlusion (MCAO) model, the APEX signal shows different spatial and temporal patterns with large inter-animal variations compared to APT and water diffusion maps. Because of the similarity between the chemical exchange saturation transfer (CEST) and SL techniques, APEX contrast can also be obtained by a CEST approach using similar irradiation parameters. APEX may provide useful information for many diseases involving a change in levels of proteins, peptides, amino-acids, or pH, and may serve as a sensitive neuroimaging biomarker.

Introduction

The chemical exchange (CE) effect has recently been exploited as a powerful sensitivity enhancement mechanism in magnetic resonance imaging (MRI). With the CE effect, low concentration agents with exchangeable protons can be indirectly detected by their effect on the water signal (Zhou and van Zijl, 2006). The use of endogeous agents such as metabolites, peptides and proteins for CE-derived image contrast is particularly attractive, because it can be used to probe the tissue microenvironment including tissue pH, temperature, and populations of exchangeable protons (van Zijl et al., 2007; Zhou et al., 2003). The CE contrast depends on the exchange rate of the labile protons with water (k), the difference in the Larmor frequencies of the two exchanging species (δ), and the populations of the exchangeable protons. While many of the early CE studies targeted the slow chemical exchange regime ($k<<\delta$) found with amide protons in proteins and peptides (Sun et al., 2005, 2007; Zhou et al., 2004), there are other endogeneous labile protons from amine, imino, and hydroxyl groups that exchange with water in the intermediate ($k\sim\delta$) or fast ($k\gg\delta$) exchange regimes that can provide CE contrast (Jin et al., 2011; Ling et al., 2008; McMahon et al., 2008; Singh et al., 2011; van Zijl et al., 2007). Specifically, exposed amine protons from free amino acids, or protein and peptide side chains are abundant in cells and exchange rapidly with water. Since these molecules are critical for life and have many functions in metabolism, image contrast from amine–water proton exchange may potentially provide valuable information about the tissue microenvironment, microstructure, or the metabolic status, and could potentially serve as sensitive biomarker for many diseases.

Biologically important molecules and macromolecules have a wide spectrum of exchangeable protons with different NMR chemical shifts and exchange rates; thus, a technique capable of selectively imaging different CE agents is desirable. It is well known that spin-locking (SL) contrast can be tuned to molecular fluctuations with different correlation times by adjusting the spin-locking frequency. Therefore, SL may serve as a versatile technique for tuning image contrast to CE agents with different exchange rates, such as slow exchanging amide or fast exchanging amine protons. Many of the current CE imaging studies employ the chemical exchange saturation transfer (CEST) technique (Ward et al., 2000). CEST, similar to off-resonance SL, can be

* Corresponding author at: Department of Radiology, University of Pittsburgh, 3025 E Carson Street, Room 156, Pittsburgh, PA, 15203, USA. Fax: +1 412 383 6799.
E-mail address: taj6@pitt.edu (T. Jin).

1053-8119/$ – see front matter © 2011 Elsevier Inc. All rights reserved.
doi:10.1016/j.neuroimage.2011.08.014

Please cite this article as: Jin, T., et al., Magnetic resonance imaging of the Amine–Proton EXchange (APEX) dependent contrast, NeuroImage (2011), doi:10.1016/j.neuroimage.2011.08.014

considered an approximation of SL when the irradiation frequency ω_1 ($=\gamma B_1/2\pi$) is much smaller than the chemical shift δ. Theoretically, SL always has a higher signal-to-noise ratio than CEST (Jin et al., 2011), and the difference in sensitivity will increase when a higher irradiation power is necessary to detect fast exchange. Another advantage of the SL approach is that the CE effect can be modeled quite well under the asymmetric population approximation developed by Trott and Palmer (Trott and Palmer, 2002). Current CEST models are based on steady-state solutions and cannot quantify intermediate or fast exchange processes (van Zijl et al., 2007). On the contrary, the dynamic evolution of water magnetization can be derived analytically using the SL model, which allows an accurate optimization of experimental parameters for enhanced sensitivity.

In this work, we aimed to detect the CE contrast from amine-proton exchange (APEX), and to show that in vivo CE contrast can be tuned to APEX or the slower amide-proton transfer (APT) by adjusting irradiation parameters, namely, the Rabi frequency (ω_1) and the duration of the SL pulse. In previous CEST applications for slow exchange, the CE sensitivity was maximized at the steady state with a low power and long irradiation pulse. When a much higher SL frequency is necessary to tune to faster exchanging protons, steady-state irradiation is no longer optimal, as will be shown below. A scheme to optimize the CE contrast for the intermediate to fast exchange regimes in the transient state is developed. Off-resonance SL experiments were performed on amino-acid phantoms and protein phantoms to examine the optimal irradiation parameters for the APEX approach. The sensitivity of APEX to protein concentration and pH changes for brain-mimicking phantoms is shown. Finally, a potential in vivo application of the APEX signal is demonstrated and compared to the APT approach using a cardiac arrest model and a focal ischemia model in rats.

Theory

Spin locking

In an SL experiment, an on-resonance excitation pulse initially flips the water magnetization away from the Z-axis by an angle θ (Fig. 1A), and then a spin-locking radiofrequency (RF) pulse is immediately applied with a transmitter frequency of Ω and a Rabi frequency of ω_1. For simplicity, the water resonance frequency is used as a reference ($\Omega=0$). The effective magnetic field $B_{1,\mathrm{eff}}$ equals $2\pi\sqrt{\Omega^2+\omega_1^2}/\gamma$ in the rotating frame, where γ is the gyromagnetic ratio (Fig. 1B). When $\theta=\arctan(\omega_1/\Omega)$, $B_{1,\mathrm{eff}}$ is collinear with the water magnetization in the rotating frame (Santyr et al., 1994). The water magnetization is then "locked" by the SL pulse and will decay with a time constant $T_{1\rho}$, the spin–lattice relaxation time in the rotating frame, to a steady state. The relaxation rate $R_{1\rho}$ ($=1/T_{1\rho}$) can be expressed as

$$R_{1\rho} = R_1\ cos^2\theta + R_2\ sin^2\theta, \tag{1}$$

where R_1 is the longitudinal relaxation rate of water and R_2 is the intrinsic water transverse relaxation rate. The magnetization at a spin-locking time (TSL), with repetition time (TR) $\rightarrow\infty$, is

$$M = (M_0 - M_{SS})\cdot e^{-R_{1\rho}\cdot TSL} + M_{SS}. \tag{2}$$

The x, y, and z component of the steady-state magnetization M_{SS} can be determined from the steady-state Bloch Equations:

$$\begin{aligned}
\frac{dM_{x,SS}}{dt} &= -R_2 M_{x,SS} + \Omega M_{y,SS} = 0\\
\frac{dM_{y,SS}}{dt} &= -\Omega M_{x,SS} - R_2 M_{y,SS} + \omega_1 M_{z,SS} = 0\\
\frac{dM_{z,SS}}{dt} &= -\omega_1 M_{y,SS} + R_1\left(M_0 - M_{z,SS}\right) = 0
\end{aligned} \tag{3}$$

which yields,

$$\begin{aligned}
M_{x,SS} &= M_0\cdot\frac{R_1\ \sin\theta\ \cos\theta}{R_2\ sin^2\theta + R_1(\ cos^2\theta + A)}\\
M_{y,SS} &= M_0\cdot\frac{R_1\ \sin\theta\cdot\sqrt{A}}{R_2\ sin^2\theta + R_1(\ cos^2\theta + A)}\\
M_{z,SS} &= M_0\cdot\frac{R_1\left(\ cos^2\theta + A\right)}{R_2\ sin^2\theta + R_1(\ cos^2\theta + A)}
\end{aligned}$$

where $A\equiv\frac{R_2^2}{\omega_1^2+\Omega^2}$, and $\tan\theta=\frac{\omega_1}{\Omega}$. Under the assumption that $A\rightarrow 0$, the above solutions can be simplified as:

$$\begin{aligned}
M_{x,SS} &\approx M_0\cdot\frac{R_1\ \sin\theta\ \cos\theta}{R_{1\rho}}\\
M_{y,SS} &\approx 0\\
M_{z,SS} &\approx M_0\cdot\frac{R_1\ cos^2\ \theta}{R_{1\rho}}.
\end{aligned} \tag{4}$$

Hence, the steady-state magnetization is

$$M_{SS} = \sqrt{M_{x,SS}^2 + M_{y,SS}^2 + M_{z,SS}^2} \approx M_0\cdot\frac{R_1\ \cos\theta}{R_{1\rho}}. \tag{5}$$

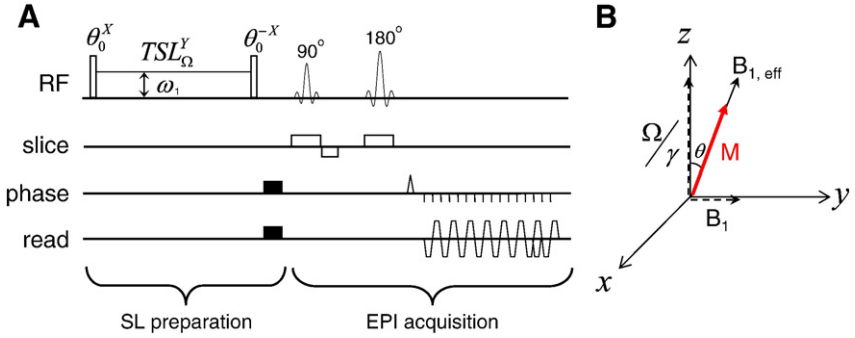

Fig. 1. Pulse sequence diagram and spin dynamics for SL experiments. (A): The pulse sequence contains an irradiation preparation and a spin-echo EPI acquisition where the super- and sub-scripts of an RF pulse denote its phase and transmitter frequency, respectively. The water magnetization is first flipped by a θ pulse and then locked by an SL pulse with frequency offset Ω, a Rabi frequency of ω_1 and spin-locking time (TSL). Following the SL pulse, the θ pulse flips the magnetization back to the Z-axis for imaging. (B): In the rotating frame, the water magnetization M is flipped to the $B_{1,\ \mathrm{eff}}$ direction by the first θ pulse and spin-locked by $B_{1,\ \mathrm{eff}}$ during TSL.

Please cite this article as: Jin, T., et al., Magnetic resonance imaging of the Amine–Proton EXchange (APEX) dependent contrast, NeuroImage (2011), doi:10.1016/j.neuroimage.2011.08.014

Spin-locking with chemical exchange

Endogenous exchangeable protons, including amide and amine groups, may be indirectly detected with CE-sensitive SL MRI. Assuming two exchangeable proton pools with highly unequal populations — i.e. $p_A \gg p_B$ where p_A and p_B are the relative populations of the water and labile protons ($p_A + p_B = 1$), respectively, and $R_2 - R_1 \ll k$ — Trott and Palmer (2002) reported that the relaxation rate, $R_{1\rho}$, can be expressed as:

$$R_{1\rho} = R_1 \cos^2\theta + (R_2 + R_{ex}) \sin^2\theta, \tag{6}$$

where

$$R_{ex} \approx \frac{p_B \cdot \delta^2 \cdot k}{(\delta - \Omega)^2 + \omega_1^2 + k^2}, \tag{7}$$

and δ and k are the chemical shift and exchange rate between the labile proton and water, respectively. R_{ex} peaks when the SL pulse is applied at the Larmor frequency of the labile proton ($\Omega = \delta$),

$$R_{ex}(\omega_1) = \frac{p_B \cdot k}{(\omega_1 / \delta)^2 + (k/\delta)^2} \tag{8}$$

In a R_{ex} vs. k plot, the maximum R_{ex} occurs at $\omega_1 = k$. This equation illustrates that when multiple chemical exchange agents with different exchange rates exist, the CE effect can be tuned to a specific exchange rate by adjusting ω_1 in an off-resonance SL experiment, i.e. ω_1-tuning (Jin et al., 2011).

Similar to CEST, SL experiments can be performed with varied Ω to get a Z-spectrum. To this end, a spin-locking ratio (*SLR*), similar to the magnetization transfer ratio used in CEST, can be defined (Jin et al., 2011). Although the name Z-spectrum refers to a Z-component of the magnetization rather than the full magnetization in SL, the term is used due to the similarity in the spectra. *SLR* can be directly obtained from Eqs. (2) and (5), noting that the $R_{1\rho}$ now contains the exchange term (R_{ex}) of Eq. (7):

$$SLR(\Omega) \equiv \frac{M(\Omega)}{M_0} = \left(1 - \frac{R_1 \cos\theta}{R_{1\rho}}\right) \cdot e^{-R_{1\rho} \cdot TSL} + \frac{R_1 \cos\theta}{R_{1\rho}}, \tag{9}$$

In our previous paper (Jin et al., 2011), the *SLR* was incorrectly expressed with $\cos^2\theta$ instead of the $\cos\theta$ term (in Eqs. (7)–(8) in Jin et al., 2011); the error is negligible for small θ, but would be significant for large θ. In a Z-spectrum, non-CE contributions such as the magnetization transfer effect from the semi-solid macromolecules are usually assumed to be symmetric around the water resonance, hence CE contrast in MRI can be conveniently assessed by the difference in two images — one acquired with off-resonance irradiation Ω on the labile proton of interest and the other as a control with opposite offset frequency from the water, $-\Omega$ (Jin et al., 2011; Zhou et al., 2003),

$$SLR_{asym}(\Omega) = SLR(-\Omega) - SLR(\Omega). \tag{10}$$

Optimization of TSL

Considering a small change of $R_{1\rho}$ induced by a variation in k or p_B, the resulting change in *SLR* would be:

$$\Delta SLR = \left\{ \left[\frac{R_1 \cos\theta}{R_{1\rho}^2} - \left(1 - \frac{R_1 \cos\theta}{R_{1\rho}}\right) \cdot TSL \right] \cdot e^{-R_{1\rho} \cdot TSL} - \frac{R_1 \cos\theta}{R_{1\rho}^2} \right\} \cdot \Delta R_{1\rho}. \tag{11}$$

To find an optimal *TSL*, the condition $\frac{\partial \Delta SLR}{\partial TSL} = 0$ leads to:

$$-\left(1 - \frac{R_1 \cos\theta}{R_{1\rho}}\right) \cdot e^{-R_{1\rho} \cdot TSL} - \left[\frac{R_1 \cos\theta}{R_{1\rho}^2} - \left(1 - \frac{R_1 \cos\theta}{R_{1\rho}}\right) \cdot TSL \right] \cdot R_{1\rho} \cdot e^{-R_{1\rho} \cdot TSL} = 0,$$

which gives an optimal *TSL* for a certain ω_1:

$$\begin{aligned} TSL_{optimal}(\omega_1) &= \frac{1}{R_{1\rho} - R_1 \cos\theta} \\ &= \frac{1}{(R_2 + R_{ex}) \sin^2\theta - R_1 \cos\theta(1 - \cos\theta)} \end{aligned} \tag{12}$$

$TSL_{optimal}$ is highly dependent on θ. In the special case of $\theta = \pi/2$ for an on-resonance SL experiment, $TSL_{optimal} = 1/R_{1\rho} = T_{1\rho}$. In the slow exchange regime, usually $\omega_1 \ll \Omega$ or $\theta \to 0$, $TSL_{optimal} \to \infty$, the contrast is optimized at the steady state (Zhou et al., 2004). Because $\sin^2\theta > \cos\theta\,(1 - \cos\theta)$ and $R_2 \gg R_1$ for in vivo applications,

$$TSL_{optimal} \approx \frac{1}{(R_2 + R_{ex}) \sin^2\theta}. \tag{13}$$

When $0 < \theta < \pi/2$, optimal *TSL* of an off-resonance SL experiment is dependent on water R_2 and R_{ex}, thus it is also dependent on the exchanging parameters such as the labile proton concentration and exchange rate.

Materials and methods

Overall MR experiments

All MRI experiments were performed on a 9.4-T/31 cm magnet with an actively-shielded 12-cm gradient insert (Magnex, UK), interfaced to a Unity INOVA console (Varian). Before the SL experiments, a T_1 map was obtained using an inversion-recovery sequence, and the B_1 field was mapped for calibration of the transmit power (Jin and Kim, 2010). The pulse sequence for SL is shown in Fig. 1A. A continuous wave SL pulse with Rabi frequency of ω_1 and duration of *TSL* was applied at the frequency offset Ω (water resonance is denoted as 0). There were two additional on-resonance pulses; the θ_0^x pulse flips the water magnetization from Z-axis to $B_{1,eff}$ direction for spin-locking, and the θ_0^{-x} pulse flips the magnetization back to Z-axis after SL for imaging. The flip angle was adjusted by changing the pulse duration of the calibrated B_1. When ω_1 and Ω were varied, the corresponding flip angle was also changed as $\theta = \arctan(\omega_1/\Omega)$. After the SL preparation, crushing gradients were applied to suppress residual transverse magnetization, and then the images were acquired with a single-shot spin-echo (SE) Echo Planar Imaging (EPI) sequence with a matrix size of 64×64. With all SL experiments, control images were measured with a 300 ppm offset to obtain M_0 (in Eq. (9)) for the calculation of the *SLR* and SLR_{asym}. In phantom experiments, B_0 maps were measured using a gradient-echo EPI with multiple echo times; for in vivo studies, water saturation shift referencing (WASSR) images were acquired to evaluate the spatial variation of B_0 field (Kim et al., 2009).

Phantom experiments

Four phantom experiments were performed at room temperature (see below). All chemicals were purchased from Sigma Aldrich (St. Louis, MO, USA). A 38-mm inner diameter volume coil (Rapid Biomedical, Ohio) was used for RF transmit and reception. Magnetic field homogeneity was optimized by localized shimming to yield a water spectral linewidth that was typically 5–10 Hz. Multiple cylinders (I.D. = 8.9 mm) were bundled together for imaging, with a field of view (FOV) of 40 mm × 40 mm. Images were collected with a slice thickness = 5 mm, and TR = 15 s. Off-resonance SL images were acquired

Please cite this article as: Jin, T., et al., Magnetic resonance imaging of the Amine–Proton EXchange (APEX) dependent contrast, NeuroImage (2011), doi:10.1016/j.neuroimage.2011.08.014

with varied TSL, Ω, and ω_1. For data analysis, a region of interest (ROI) with minimal B_0 heterogeneity (<3 Hz) was selected from each sample.

Phantom experiment I

To examine the dependence of optimal *TSL* on labile proton concentration, 30 mM or 60 mM Glutamate (Glu) was dissolved in Phosphate Buffered Sulfate (PBS), and titrated to pH = 6.9. To examine the effect of water R_2 to APEX contrast, two 30 mM Glu phantoms were prepared in PBS (pH = 6.9), one contained 0.15 mM $MnCl_2$ and the other contained 2% agarose. For agar phantoms, the mixture was initially heated to 90–95 °C in a water bath for 2–3 min, and then cooled down to 60 °C and transferred to a plastic cylinder to solidify. The chemical shift between Glu amine and water protons is 3 ppm, and their exchange rate at pH = 6.9 is about 4350 s^{-1} (Jin et al., 2011). Off-resonance SL spectra at Ω of +3 ppm and −3 ppm were acquired with varied *TSL* between 0 and 3 s and ω_1 between 190 and 750 Hz. SLR_{asym} at 3 ppm was calculated using Eq. (10) as a function of *TSL* and ω_1. Also, optimal *TSL*, which maximizes the SLR_{asym}, was obtained at each ω_1. To determine the intrinsic water R_2, the on-resonance $R_{1\rho}$ was measured with $\omega_1 = 4000$ Hz, since the CE effect is minimized in the on-resonance $R_{1\rho}$ with such high SL power (i.e., $R_{ex} \approx 0$ and $\theta = 90°$ in Eqs. (6) and (7)).

Phantom experiment II

To evaluate whether the APEX signal has a significant contamination from the effect of hydroxyl-water proton exchange, 30 mM Glu together with 10 mM myo-inositol (Ins) were dissolved in PBS with 0.15 mM $MnCl_2$ added, and then titrated to pH = 6.9. The chemical shift of myo-inositol hydroxyl proton is less than 1 ppm from water. The 10 mM Ins was chosen because this would be similar to the in vivo concentration of hydroxyl protons from brain metabolites. 2% Agar and PBS phantoms without metabolites were also measured as controls. The experimental parameters used here were same as in Phantom experiment I.

Phantom experiment III

To validate that APEX is sensitive to protein concentration, 0.5, 1, 2, or 3% (by weight) bovine serum albumin (BSA) was added to PBS (pH = 7.4). Z-spectra were acquired on the 4 phantoms with a low power and long irradiation pulse (85 Hz and 5 s), and a high-power and short pulse (500 Hz and 1.5 s).

Phantom experiment IV

To examine the APEX sensitivity to pH, brain-mimicking phantoms were prepared at pH values of 5.8, 6.3, 6.9 and 7.4. Each phantom contained 10 mM Glu, 10 mM Taurine, 10 mM Glutamine and 4% (by weight) BSA in PBS, 0.06 mM $MnCl_2$ was added to the solutions to shorten T_1 and T_2 ($R_1 = 0.7$ s^{-1} and $R_2 = 5.4$ s^{-1}). The SLR_{asym} at 2.75 ppm was measured for ω_1 of 125, 250, 500 and 1000 Hz, and *TSL* of 0 to 4 s. The optimal *TSL* which maximizes the SLR_{asym} for these ω_1 values was 4 s, 2 s, 0.7 s, and 0.35 s, respectively. Then, Z-spectra were acquired with ω_1 of 125 Hz at *TSL* of 4 s, 250 Hz at 2 s, 500 Hz at 0.7 s, and 1000 Hz at 0.35 s. The peak SLR_{asym} data of each ω_1 were fitted by a Lorentzian function.

Rat experiments for cardiac arrest and stroke models

Rat preparation

Cardiac arrest, and focal brain ischemia experiments were performed with approval from the Institutional Animal Care and Use Committee at the University of Pittsburgh. Fourteen male Sprague–Dawley rats (weighing from 320–420 g) were anesthetized with isoflurane (5% for induction and 2% during surgery) via a vaporizer with a mixture of O_2 (30%) and N_2 (70%). The femoral vein was cannulated to deliver pancuronium bromide (0.2 mg/kg/h) and maintenance fluid. The femoral artery was catheterized to monitor the arterial blood pressure and to obtain blood samples for arterial blood gas measurements. For focal ischemia studies (n = 7), the middle cerebral artery occlusion model (MCAO) was adapted (Kiozumi et al., 1986). In short, an incision was made on the midline of the neck. The left common carotid artery (CCA), internal carotid artery (ICA), and external carotid artery (ECA) were isolated and the CCA and ECA ligated. A 4–0 monofilament nylon suture coated with silicon rubber (Doccol Corp., CA, USA) was inserted from the ECA into the ICA to occlude the origin of the middle cerebral artery (MCA). During MRI experiments, the isoflurane level was reduced to 1.3–1.5%. The dynamic blood pressure and end-tidal CO_2 were monitored. End-tidal CO_2 level was kept within 3.5 ± 0.5%, and the rectal temperature was controlled at 37.2 ± 0.5 °C using a water circulating pad.

Cardiac arrest (total n = 7 animals)

In vivo Z-spectra were obtained (n = 4 animals) using a surface coil to optimize the APEX contrast at baseline and also to compare with data collected post-mortem. The FOV was 2.56 cm × 2.56 cm, the slice thickness was 4 mm, and TR was 9 s. The surface coil enhances the sensitivity, but has B_1 spatial heterogeneity; therefore, only a small ROI at the cortex, where B_1 is relatively homogeneous was selected (see below). Both the B_1 calibration for SL and data analysis was performed on this cortical ROI. Before the cardiac arrest, in vivo Z-spectra were measured with eight different SL pulse powers and durations: 44 Hz for 4 s; 63, 88, and 125 Hz for 2 s; 175 and 250 Hz for 300 ms; 350 Hz for 200 ms; and 500 Hz for 150 ms. The postmortem measurements were performed with 63 Hz for 2 s and 500 Hz for 150 ms between 30 min to 90 min after cardiac arrest was induced by an intravascular bolus injection of saturated KCl (0.5–0.8 ml). Z-spectra were measured within 10 to −10 ppm range. After cardiac arrest, the post-mortem body temperature drops and the water resonance frequency drifts at a rate of −0.01 ppm/°C (Hindman, 1966). Because SLR_{asym} closer to the water resonance frequency is more susceptible to the frequency shift, Z-spectra were acquired with a center-out order: 0, ±0.2 ppm, ±0.4 ppm, etc., to reduce the contamination caused by frequency drift during each scan. To evaluate the image contrast in cortex, subcortical area, and white matter, the APT-weighted image and APEX image were acquired before and after cardiac arrest (n = 3 animals), with a volume coil transmit and surface coil reception setup (Nova Medical, MA, USA). The FOV was 2.56 cm × 2.56 cm, the slice thickness was 2 mm, and TR was 6 s. APT-weighted images were measured with Ω = ±3.5 ppm, $\omega_1 = 63$ Hz, and *TSL* = 3 s, and the APEX images were measured with Ω = ±2.5 ppm, $\omega_1 = 500$ Hz, and *TSL* = 150 ms.

MCAO model (n = 7 animals)

A volume coil was used for transmit and a surface coil was used for reception. The FOV was 2.56 cm × 2.56 cm, the slice thickness was 2 mm, and TR was 6 s. Apparent water diffusion coefficient (ADC), APT-weighted, and APEX maps were measured at 1, 2, 3, and 4 h after the MCA occlusion, and T_2 maps were measured at the 1st and 4th hour. ADC maps were obtained using a multi-slice SE EPI sequence, with a low *b*-value of 5 s/mm^2 applied on one axis, and a high *b*-value of 1200 s/mm^2 applied on six different directions. For APT, single-slice images were acquired at offset = ±3.5 ppm and 300 ppm with an irradiation power of 63 Hz for 3 s. For APEX, single-slice images were acquired at offset = ±2.5 ppm and 300 ppm with an irradiation power of 500 Hz for 150 ms. Since the B_0 heterogeneity determined from the WASSR scan was relatively small (typically less than 0.04 ppm) in the imaging slice, no B_0 correction was performed for the APEX and APT images in this preliminary study.

Results

Phantom experiments

The effect of ω_1, concentration of metabolite, and water R_2 on APEX contrast was determined in Phantom experiment I. SLR_{asym} at 3 ppm

Please cite this article as: Jin, T., et al., Magnetic resonance imaging of the Amine–Proton EXchange (APEX) dependent contrast, NeuroImage (2011), doi:10.1016/j.neuroimage.2011.08.014

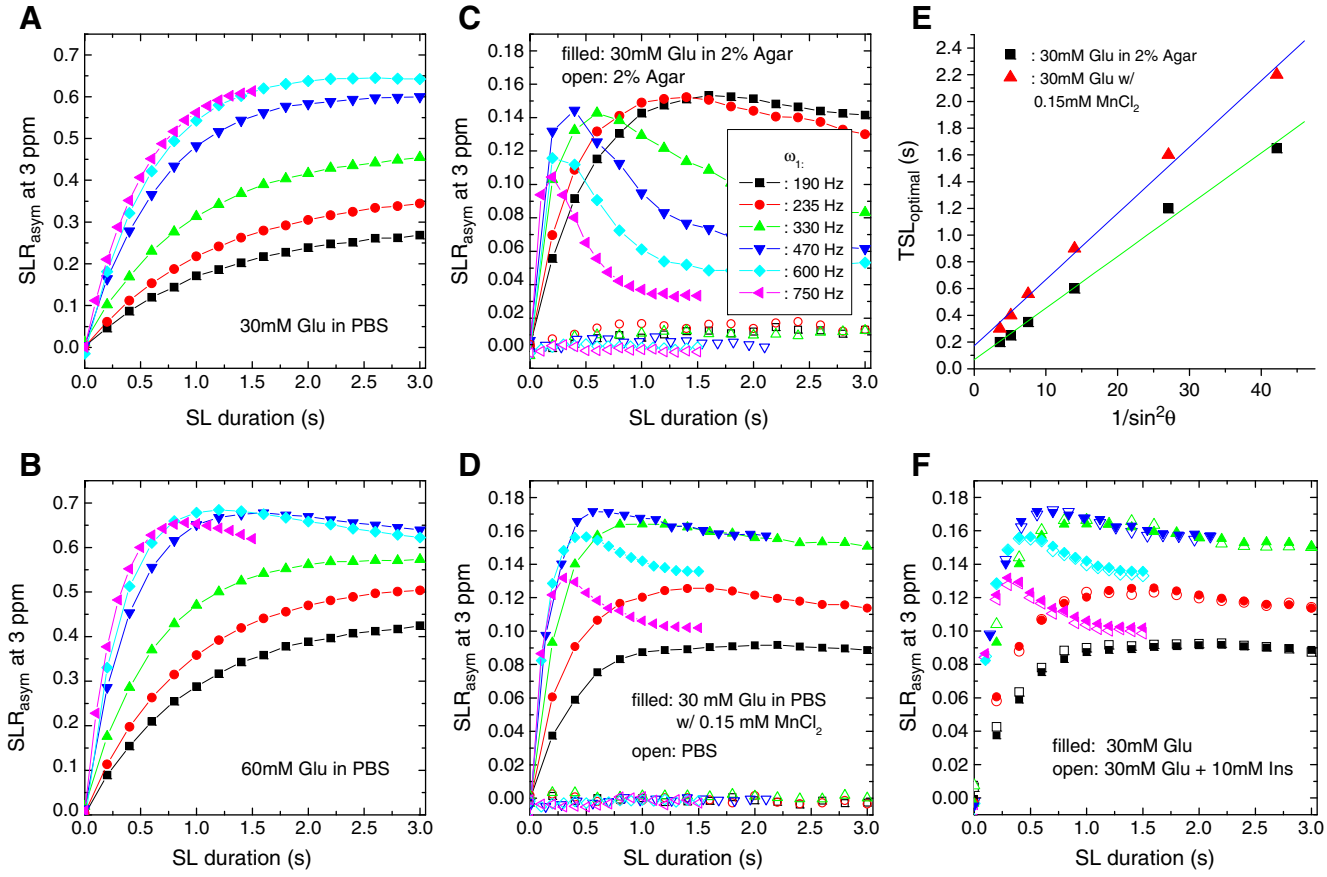

Fig. 2. APEX contrast of glutamate with different concentration and water R_2. SLR_{asym} as a function of *TSL* was measured for several ω_1 values at 3 ppm for 30 mM Glu in PBS (A), 60 mM Glu in PBS (B), 30 mM Glu in 2% agar (C), and 30 mM Glu in PBS with 0.15 mM $MnCl_2$ (D). 2% agar alone had very small SLR_{asym} (open symbols, C) whereas PBS had no detectable SLR_{asym} (open symbols, D). For 30 mM Glu in either 2% agar or in PBS with 0.15 mM $MnCl_2$, the optimal *TSL* values that maximize the SLR_{asym} are approximately linearly dependent on $1/\sin^2\theta$ (E), which can be also predicted by Eq. (13). At 3 ppm, there were little differences in SLR_{asym} for 30 mM Glu with and without the addition of 10 mM of myo-inositol (F). The symbol representation of irradiation power in the inset of (C) applied to all other panels except (E).

was measured on the four glutamate phantoms, as shown in Figs. 2A–D. For the 30 mM Glu sample in PBS with a water R_2 of ~0.5 s^{-1} (Fig. 2A), the APEX contrast increased with *TSL* in the *TSL* <3 s range, and was maximized at an ω_1 of ~600 Hz, which is much higher than the power levels used for slower chemical exchange rates (~100 Hz or less). With the higher Glu concentration of 60 mM, the $TSL_{optimal}$ started to decrease for $\omega_1 \geq 470$ Hz (Fig. 2B), and the maximum SLR_{asym} was reached at $TSL = 1.2$ s for ω_1 of 600 Hz. For 30 mM Glu in 2% agar with a water R_2 of ~16.2 s^{-1} (Fig. 2C) or in 0.15 mM $MnCl_2$ with a water R_2 of ~12.2 s^{-1} (Fig. 2D), the SLR_{asym} was greatly reduced due to the increased R_2 (compared to Fig. 2A), and the shift of $TSL_{optimal}$ became more obvious. For the same ω_1, the peak SLR_{asym} shifted to a shorter *TSL* with a higher metabolite concentration (Fig. 2A vs. B), or with a larger R_2 value (Fig. 2A vs. 2C and 2D). For 30 mM Glu phantoms in 2% agar or with 0.15 mM $MnCl_2$, the experimentally-determined $TSL_{optimal}$ for each ω_1 was plotted against $1/(\sin^2\theta)$. Both data sets show roughly linear dependence (Fig. 2E), as expected from Eq. (13); the larger θ induced by a higher ω_1 (smaller number in the X axis) requires a smaller $TSL_{optimal}$ value for maximizing the CE contrast.

Phantom experiment II evaluated the effect of hydroxyl-water proton exchange on APEX signal for a 30 mM Glu sample with 10 mM myo-inositol (open symbols, Fig. 2F). Compared to the SLR_{asym} of the 30 mM Glu sample without Ins (filled symbols), the difference was very small and within experimental error. While the PBS results had negligible SLR_{asym}, as expected (open symbols, Fig. 2D), the 2% agar phantom showed a small SLR_{asym} of 1–2% for $\omega_1 \leq 330$ Hz (open symbols, Fig. 2C), and an SLR_{asym} of less than 1% for $\omega_1 \geq 470$ Hz. This small SLR_{asym} may be due to proton exchange between agarose hydroxyls and water. Nevertheless, our phantom data indicates that the contamination to APEX signal from hydroxyl–water proton exchange should be quite small.

We examined the dependence of protein concentration on the APEX contrast in Phantom Experiment III (Fig. 3). The SL Z-spectra of four BSA samples with different concentrations are plotted in Fig. 3A for a low-power and long irradiation pulse ($\omega_1 = 85$ Hz and $TSL = 5$ s) and in Fig. 3B for a high-power and short irradiation pulse ($\omega_1 = 500$ Hz and $TSL = 1.5$ s). In SL Z-spectra, the signal dipped at about 2–3 ppm due to the CE effect, but the dip was more significant with the high power pulse of 500 Hz. It should be noted that a small dip was also seen around −3 ppm with low power irradiation (see upward arrow), which may be due to the Nuclear Overhauser Effect (NOE), i.e. cross-relaxation between water and side chains of macromolecules (Chen et al., 2006; Ling et al., 2008). Unlike CEST Z-spectra, where the magnetization vanishes at the water resonance frequency due to direct water saturation, the SL Z-spectra did not go to zero with a 1.5-s spin-locking pulse especially for the lower concentration samples, because the signal decay is slow with the long on-resonance $T_{1\rho}$ for these aqueous samples. SLR_{asym} peaks centered at around 2.5 ppm were seen with both the low (dashed lines) and high irradiation powers (solid lines), but the magnitude was much larger with the high power irradiation (Fig. 3C). The peaks were relatively broad, suggesting fast chemical exchange between BSA labile protons and water. The magnitude of SLR_{asym} was almost linearly dependent on the BSA concentration between 0.5 to 2%, but not for the higher 3% concentration.

Recent studies have examined the pH-dependence of amine-water proton exchange for Glutamate (Jin et al., 2011; Singh et al., 2011). In

Please cite this article as: Jin, T., et al., Magnetic resonance imaging of the Amine–Proton EXchange (APEX) dependent contrast, NeuroImage (2011), doi:10.1016/j.neuroimage.2011.08.014

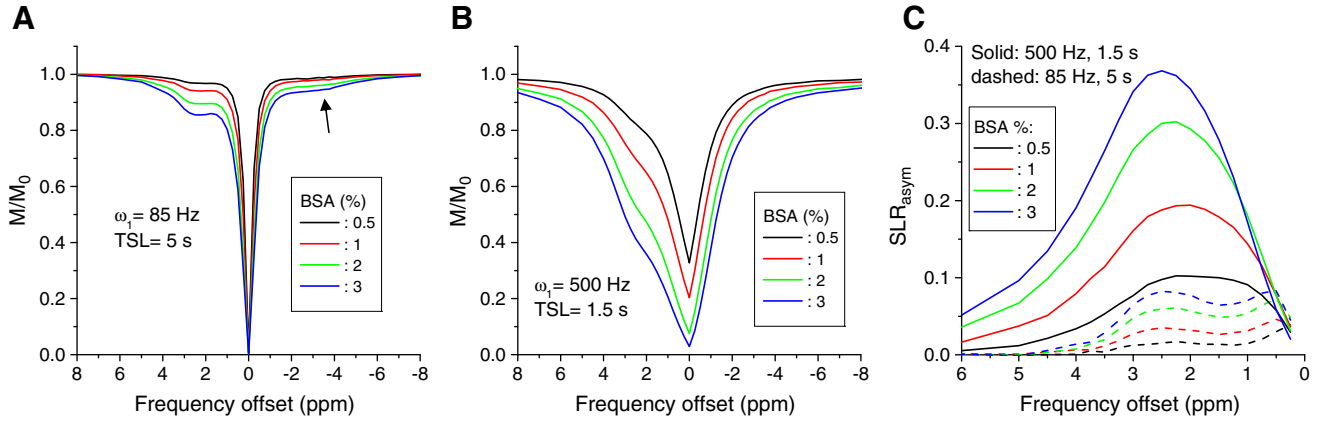

Fig. 3. APEX contrast of bovine serum albumin proteins with different concentration. Z-spectra of BSA phantoms were measured with a SL frequency of 85 Hz and *TSL* of 5 s (A), and with a higher SL frequency of 500 Hz and a shorter *TSL* of 1.5 s (B). The NOE effect can be seen with a long irradiation time (arrow in A). The SLR_{asym} peaks were quite broad due to the fast exchange rates, and are more prominent with high irradiation power (C).

brain, however, there are a variety of amine protons with different exchange rates and chemical shifts, therefore the measured APEX signal will be a weighted summation from all the amine groups. To mimic the APEX signal in brain, we prepared phantoms containing 4% BSA and 10 mMs of Glutamate, Glutamine, and Taurine at 4 different pH values (Phantom Experiment IV). Fig. 4 shows the effect of pH on the APEX signal in these phantoms. With $\omega_1 = 125$ Hz and $TSL = 4$ s, the SLR_{asym} was small for pH = 7.4, but increased with decreasing pH, reaching a maximum at pH = 5.8 where a peak appeared at about 3 ppm (Fig. 4A). With $\omega_1 = 500$ Hz and $TSL = 700$ ms, the maximum SLR_{asym} was reached at 2.75 ppm for the pH = 6.3 sample (Fig. 4B). Similar to amide–proton transfer, amine–water proton exchange is base-catalyzed over this pH range and the exchange rate decreases with pH. With increasing ω_1, the peak of SLR_{asym} at 2.75 ppm shifted to higher pH values, i.e., fast exchange rates (Fig. 4C), which resembles our previous simulation of off-resonance $R_{1\rho}$ (Fig. 5D in (Jin et al., 2011)). Thus, the image contrast can be tuned to specific pH conditions by changing the SL parameters (Fig. 4D). At ω_1 of 125 Hz (upper right image), the highest CE contrast occurred with the slow exchange condition, pH of 5.8. With a higher ω_1 of 500 Hz (lower left image) the contrast is optimal for a faster amine exchange rate, pH = 6.3, while for ω_1 of 1000 Hz (lower right image), the highest CE contrast was between pH of ~6.3 and 6.9.

Animal experiments: Live vs. postmortem conditions

The averaged SL Z-spectra and SLR_{asym} spectra for live animals (n = 4) are plotted in Fig. 5. The spectra were obtained from an ROI at the rat cortex (red pixels on the inset image). With low power and long irradiation pulses, which is optimized for slow chemical exchange (Fig. 5A), small dips at 3.5 ppm from amide -water proton exchange (black arrow) are clearly observed in the spectra for $\omega_1 = 44$ to 88 Hz. In addition, a large broad feature (green arrow) is seen on the opposite side in the −2 to −5 ppm range, which is more prominent for the lower irradiation power. Similar to the observation with the BSA phantoms (Fig. 3A), this may be due to the NOE and is still under investigation. For higher irradiation power and shorter pulses, the Z-spectra were smoother and broader (Fig. 5B). In vivo SLR_{asym} spectra (Fig. 5C) revealed a transition from the APT effect with a peak around 3.5 ppm (black arrow) to the APEX effect with a peak around ~2.5 ppm (blue arrow) with increasing irradiation power and decreasing pulse duration. For $\omega_1 = 44$ and 63 Hz, distinct and narrow amide peaks were well resolved at 3.5 ppm (black arrow, Fig. 5C) on top of the broad curved SLR_{asym} due to the asymmetry from conventional magnetization transfer (MT) and NOE effects. Note that the amide peak is positive, but SLR_{asym} caused by the MT asymmetry and the NOE effect is negative. When this broad SLR_{asym} baseline was removed, the magnitude of the APT peak was estimated to be ~1.7% at $\omega_1 = 63$ Hz. With increasing power to 88 and 125 Hz, the amide peak was reduced, which basically agrees with a previous report that APT contrast at 4.7 T is maximized for 0.75 to 1 μT (31 to 42 Hz) (Sun et al., 2007). When a higher power and short irradiation pulse was used (see Fig. 5C), the APEX effect dominated and the SLR_{asym} became positive, indicating that the NOE effect and the MT asymmetry are small for these parameters. The APEX signal is much broader than APT suggesting a faster exchange, because the linewidth of SLR_{asym} or more specifically R_{ex} (Eq. (7)) is correlated with the exchange rate (Jin et al., 2011). In addition, various amine-groups with different exchange rates and chemical shifts may contribute and broaden the APEX signal. The APEX peak appeared at an offset in the 2–3 ppm range, and the amplitude was about 8% for $\omega_1 = 350$ and 500 Hz (blue arrow, Fig. 5C). Overall, the in vivo APEX contrast obtained with a high power and short irradiation pulse is much larger than the APT contrast.

The sensitivity of APT and APEX contrast during global ischemia induced by cardiac arrest was compared in Fig. 6. APT contrast was obtained either with a 2-s pulse (6A) or 3-s pulse (6C) and $\omega_1 = 63$ Hz, while the APEX contrast was measured with a 0.15-s pulse and $\omega_1 = 500$ Hz. With a low power and long irradiation pulse, the difference between the live and postmortem data mostly occurred on the downfield frequency of the water resonance, where the APT peak at 3.5 ppm disappeared from the SLR_{asym} plot (black arrow, Figs. 6A and B), indicating a reduce rate of amide–proton exchange. In Z-spectra with $\omega_1 = 500$ Hz, the signal dropped in a wide offset region around the amine frequencies (2–3 ppm) also indicating a decrease in amine–proton exchange, and consequently an increase in the SLR_{asym} APEX signal (Fig. 6B), similar to the phantom APEX results with pH from 7.4 to 6.9 in Fig. 4B (lower pH induces higher APEX). The postmortem APEX peak was about 16% at $\Omega = 2.5$ to 2.75 ppm, thus the absolute increase of APEX was about 8% (~100% relative increase). Changes in SLR_{asym} at 3.5 ppm and 2.5 ppm were clearly observed in images obtained during live and postmortem conditions (Fig. 6C). In APT-weighted images (6C, bottom), negative contrast was observed and was more prominent in the corpus callosum area (red arrow) than in the cortex (green arrow), but the contrast did not change much after cardiac arrest since the change of APT is small compared to the dominant NOE and MT asymmetry effects (as seen in Fig. 6B). In contrast, the APEX map (upper row) was relatively homogeneous and showed a large increase in a postmortem.

In vivo animal experiments of stroke model

Fig. 7 shows the T_2, ADC, APT-weighted, and APEX maps for three rats at 1 h and 4 h after the occlusion of the left middle cerebral artery.

Please cite this article as: Jin, T., et al., Magnetic resonance imaging of the Amine–Proton EXchange (APEX) dependent contrast, NeuroImage (2011), doi:10.1016/j.neuroimage.2011.08.014

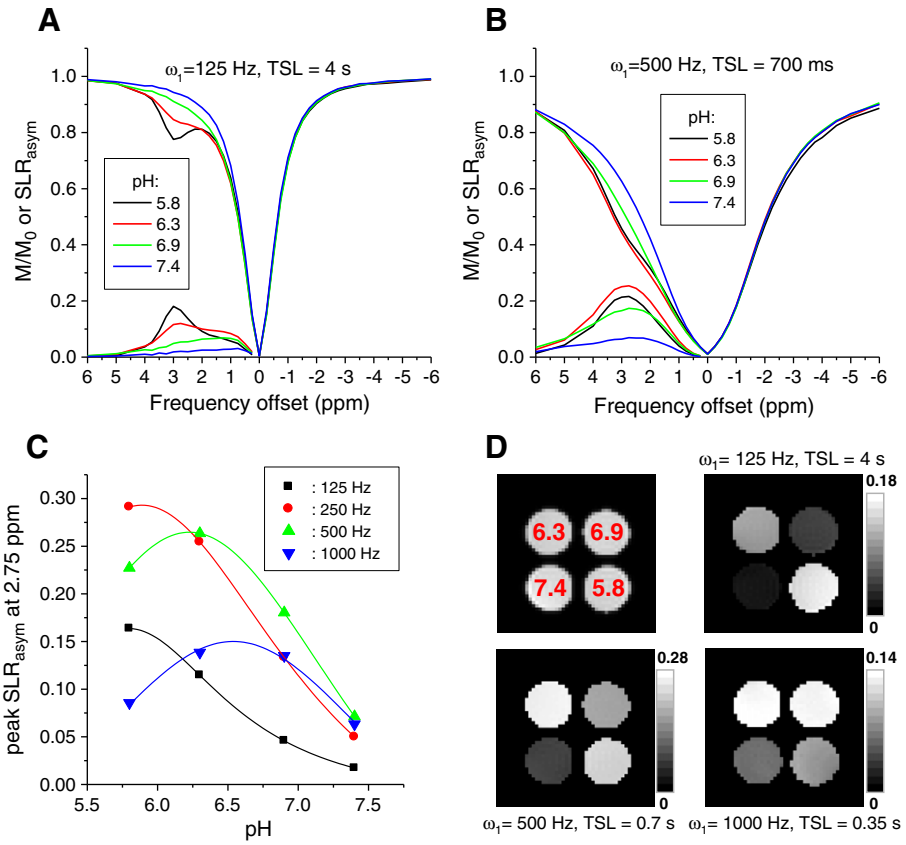

Fig. 4. APEX contrast of brain-mimicking phantoms with different pH. Brain-mimicking phantoms containing 10 mM glutamate, 10 mM taurine, 10 mM glutamine and 4 wt.% bovine serum albumin had four different pH values of 5.8, 6.3, 6.9, and 7.4. Z-spectra and SLR_{asym} of the brain-mimicking phantoms were obtained with a SL frequency of 125 Hz and *TSL* of 4 s (A), and with a higher SL frequency of 500 Hz and shorter *TSL* of 0.7 s (B). To examine pH-dependent APEX response (C), the peak of SLR_{asym} at 2.75 ppm was obtained from *TSL*-dependent data for each SL frequency. With a lower SL frequency, SLR_{asym} was tuned to lower pH sample. The lines represent a Lorentzian fit for experimental data (symbols). SLR_{asym} maps at 2.75 ppm were shown for three SL conditions (D). In addition, a corresponding spin-echo EPI image (upper left in D) is shown with pH values denoted in red. (For interpretation of the references to color in this figure legend, the reader is referred to the web version of this article.)

While T_2 maps did not show significant stroke lesions especially at the 1st hour after the occlusion, large lesions in the left hemisphere (right side in the images) were seen in the ADC, APT-weighted and APEX maps. From our data on 7 animals, APEX maps showed large spatial and temporal inter-animal variations. In 5 of the 7 animals, the APEX maps showed clearly different spatial patterns and were smaller in spatial content as compared to the ADC and APT maps, e.g. subcortical regions in rat # 1 and # 2 (arrows). Moreover, the APEX images also displayed larger temporal variations than ADC and APT; 4 rats exhibited reduced APEX signals with time (e. g., rats #1 and #3), whereas 3 others showed increased APEX signals with time (e. g., rat #2). The difference in APT signals between lesion area and the

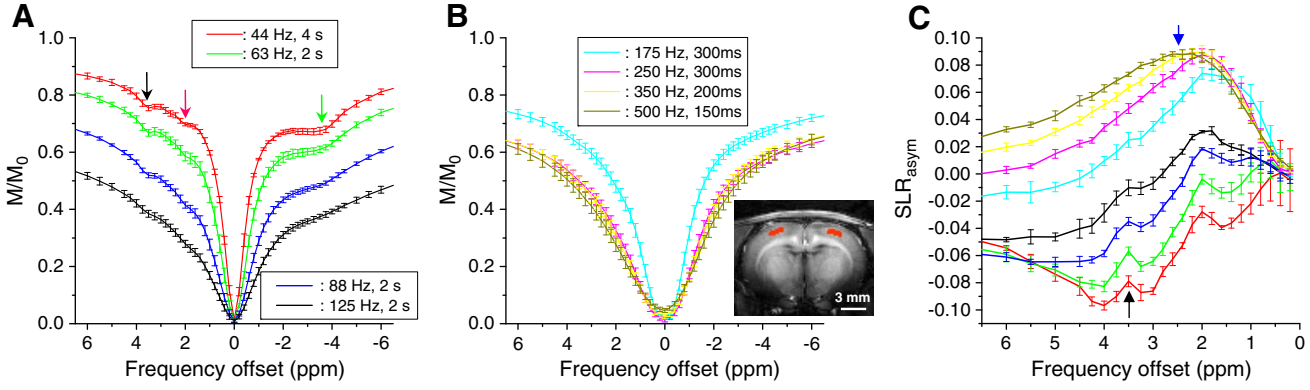

Fig. 5. *In vivo* Z-spectra and SLR_{asym} of the rat cortex. Z-spectra (A and B) and SLR_{asym} (C) were obtained from small red marked brain regions (insert image) as a function of spin-locking pulse power ω_1. With low power and long SL pulses, that are tuned to slow chemical exchange and slow molecular motions, Z-spectra showed a well-resolved signal dip at 3.5 ppm (black arrow), a smaller dip at ~2 ppm (red arrow), and a broad pronounced dip at −2.5 to −4 ppm (green arrow) on the control side of the spectra (A). With high power and short SL pulses tuned to fast chemical exchanges, the Z-spectra became smooth and broad (B). SLR_{asym} (C) showed narrow APT peak at 3.5 ppm on top of a distorted baseline due to NOE effects from the upfield control side (black arrow). With increasing pulse power and shorter irradiation duration, the APT peak was suppressed and the APEX peak, around 2.5 ppm, became more prominent (blue arrow). Error bars: standard deviations (n = 4). (For interpretation of the references to color in this figure legend, the reader is referred to the web version of this article.)

Please cite this article as: Jin, T., et al., Magnetic resonance imaging of the Amine–Proton EXchange (APEX) dependent contrast, NeuroImage (2011), doi:10.1016/j.neuroimage.2011.08.014

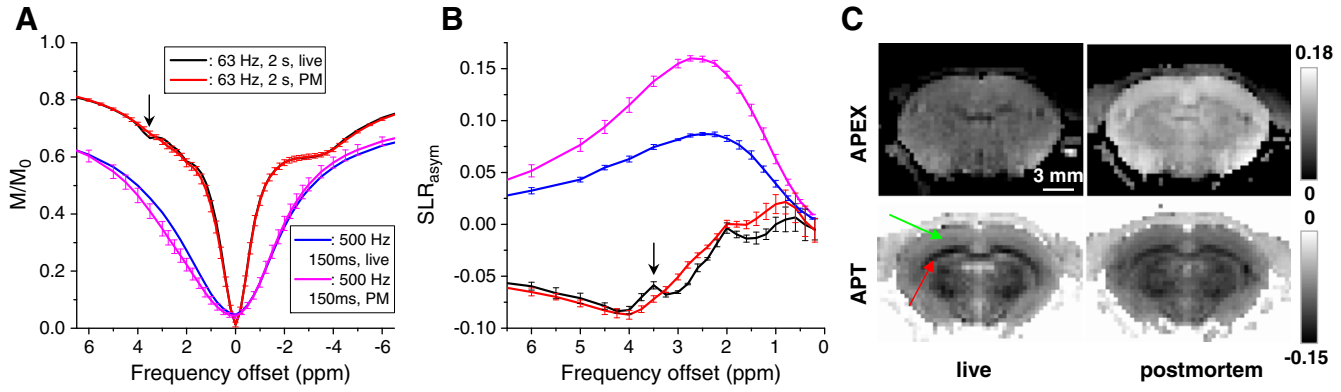

Fig. 6. Z-spectra and SLR_{asym} of live vs. postmortem rat brain. Z-spectra (A) and SLR_{asym} (B) of live and postmortem (PM) rat cortex were acquired with $\omega_1 = 63$ Hz and $TSL = 2$ s that tunes to APT, and with $\omega_1 = 500$ Hz and $TSL = 150$ ms that tunes to APEX. After cardiac arrest, the APT peak at 3.5 ppm disappeared in the Z-spectra (arrow) and also in the SLR_{asym}. In contrast, the APEX peak increased from ~8% to ~16%. (C). Error bars: standard deviations (n = 4). The APEX map (upper row) and APT-weighted maps (lower row) of live (left column) and PM rat brain (right column) showed a very different contrast. A red arrow indicates the corpus callosum, white matter, while a green arrow indicates the cortical region, gray matter. (For interpretation of the references to color in this figure legend, the reader is referred to the web version of this article.)

corresponding area at the right hemisphere was ~1.7% in the MCAO model, similar to the cardiac arrest results. While the APEX signal is ~8% at the control side, the APEX signal at the lesion region typically ranges between 9 and 14% and is both spatial- and time-dependent.

Discussion

With the SL technique, CE contrast can be tuned to different labile protons by adjusting the irradiation parameters. Slow, intermediate,

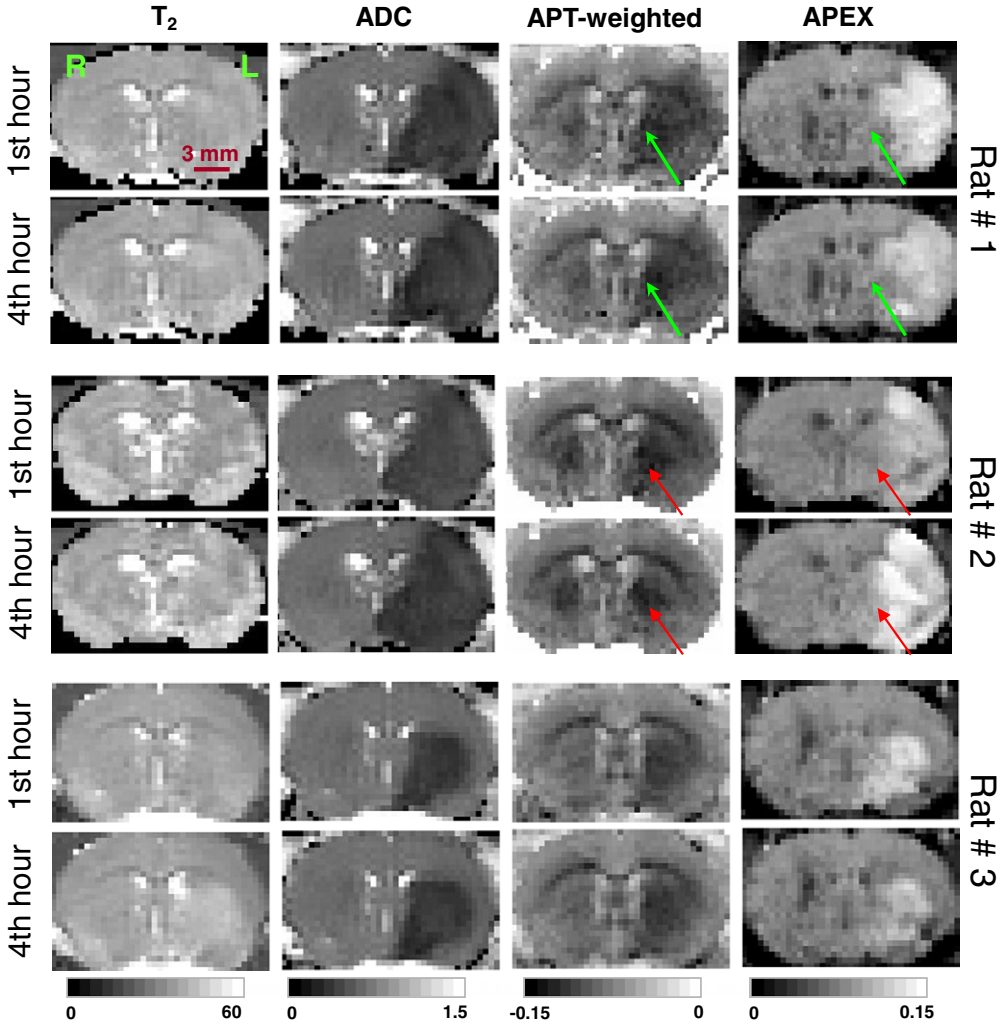

Fig. 7. Chemical exchange-sensitive maps after left middle cerebral artery occlusion. Maps of T_2, ADC, APT-weighted, and APEX were obtained on three rats at one hour (upper row) and 4 h (lower) after the onset of MCAO. APT-weighted images were acquired at offset = ±3.5 ppm with an irradiation power of 63 Hz for 3 s, while APEX images were acquired at offset = ±2.5 ppm with an irradiation power of 500 Hz for 150 ms. Different spatial and temporal patterns of the stroke lesion can be seen with the APEX maps as compared with the other maps. Arrows: mismatch between APEX and APT maps in the subcortical area. Unit of gray scales: ms for T_2, 10^{-3} mm^2/s for ADC, and SLR_{asym} for APT-weighted and APEX. R: right hemisphere; L: left hemisphere.

Please cite this article as: Jin, T., et al., Magnetic resonance imaging of the Amine–Proton EXchange (APEX) dependent contrast, NeuroImage (2011), doi:10.1016/j.neuroimage.2011.08.014

and fast exchange regimes are imaged optimally with low power and long duration, intermediate power and duration, and high power and short duration spin-locking pulses, respectively. From Eq. (7), the linewidth of R_{ex} as a function of the frequency offset Ω is equal to $\sqrt{\omega_1^2 + k^2}$. With slow exchange and low irradiation power, the R_{ex} peak is narrow so that the CE contrast can only be detected within a small offset range of the labile proton frequency ($\Omega = \delta$). Consequently, the slow-exchange sensitive CE method has high specificity, such as APT where amide proton resonance frequency is well-resolved from the water resonance. With intermediate- and fast-exchange sensitive CE contrast, high RF power and fast exchange rates reduce the specificity of CE contrast. Since the R_{ex} peak becomes broader, CE contrast can be detected at the frequency offset far away from the labile proton frequency (Jin et al., 2011). As shown in our data (Figs. 3–6), the APEX SLR_{asym} peak is much broader than the narrow peak from the APT effect, indicating a reduced specificity for APEX.

In vivo, there are a variety of amine-groups with different chemical shifts and exchange rates. For example, creatine has a much slower amine–water proton exchange rate than many amino-acids, such as glutamate (Jin et al., 2011; Sun et al., 2008). Roughly, the chemical shift between amine and water protons is 2–3 ppm (5026–7540 rad/s at 9.4 T) (Ward et al., 2000), and the amine exchange rates span a wide range between 500 s^{-1} to 10000 s^{-1} (Liepinsh and Otting, 1996; van Zijl and Yadav, 2011). Thus, the in vivo APEX signal represents a weighted summation of many different amine groups. The contribtuion to the APEX signal from a certain amine-group depends on several variables, including the chemical shift, concentration, and exchange rate which is dependent on pH and temperature, as well as experimental parameters including the power and duration of the irradiation pulse, and the frequency offset. Further study is necessary to systematically determine the amine–proton exchange rates of the protein/peptides and the different amino acids. In addition to APEX, a high power irradiation pulse may also be sensitive to other intermediate to fast CE, such as the hydroxyl–water proton exchange with exchange rates between 700 and 15000 s^{-1} (Liepinsh and Otting, 1996; Ward et al., 2000). Although some of the hydroxyl groups may be close to the amine Larmor frequencies, e.g., glucose has CEST peaks close to 2 and 3 ppm (van Zijl et al., 2007), most hydroxyl groups have much smaller chemical shift (~1 ppm) than amines; therefore, the contamination from hydroxyl–water exchange to our APEX signal should be small, which we confirmed with phantom experiment II (see Fig. 2F). Finally, the CE effect is highly dependent on the ratio of exchange rate to the chemical shift (k/δ), which will increase at lower magnetic fields. At lower fields, the frequency separation between amine and water protons is smaller so that many of the amine exchange rates may become too fast to be detected by the APEX experiment. Consequently, the APEX contrast may be smaller at 1.5 or 3 T.

At a high field of 9.4 T, the APT peak at 3.5 ppm can be well-resolved in the Z-spectra of brain due to the increased spectral resolution compared to 3 T and 4.7 T (Zhou et al., 2003). However, a pronounced broad peak around −2 to −5 ppm was also observed, which greatly distorted the baseline of SLR_{asym}. A similar result was reported in homogenized rat brain at 9.4 T (Narvainen et al., 2010). This upfield feature is not readily seen at 1.5 T and 3 T, but has been observed in humans at 7 T (Mougin et al., 2010). The exact source of this broad peak is not clear, but it is likely due to an inter/intramolecular NOE which increases slowly with irradiation time (Chen et al., 2006; van Zijl and Yadav, 2011). The observed NOE, in addition to the recently reported problem of asymmetry with the conventional MT effect (Hua et al., 2007) makes quantification of APT from the SLR_{asym} analysis challenging. The APEX contrast is obtained from the asymmetry analysis similar to APT. Since a much shorter irradiation pulse is used with APEX, the NOE contamination is smaller and the MT effect may also be less. As a result, no significant subtraction problem in SLR_{asym} was observed (as seen in Fig. 5C).

One feature of the SL technique is its ability to tune to a specific pH or exchange rate (see Fig. 4C). Note that R_{ex} in Eq. (8) peaks at $\omega_1 = k$. Hence, R_{ex} and SLR_{asym} can be tuned to a particular k by adjusting SL power to be $\omega_1 = k$ (Jin et al., 2011). Our data suggests that when the pH decreases, the exchange rate shifts from fast to intermediate for APEX, and from slow to slower for APT. Thus, the APEX contrast increases as pH decreases, while the APT contrast decreases with pH (McMahon et al., 2006). This inverse relationship between CE contrast and pH has also been observed for hydroxyl–water proton exchange with poly-L-threonine (McMahon et al., 2008). In practice, the optimization of ω_1 to achieve maximum sensitivity depends on the type of application. To detect a change of labile proton concentration with minimal variation in the exchange rate, the ω_1 that gives the maximum SLR_{asym} should be selected. In the example of Fig. 4C, that would be 250 Hz for pH = 5.8, and 500 Hz for pH = 6.3 to 7.4. Conversely, to detect a change in exchange rate without a change in the labile proton concentration, ω_1 should be selected that has the largest slope in SLR_{asym} for the pH range of interest, i.e. 250 Hz (or similarly, 500 Hz) in the example of Fig. 4C. Note that in contrast to R_{ex}, which is proportional to p_B (Eqs. (7) and (8)), SLR_{asym} does not linearly increase with the concentrations of protein or metabolites when concentrations are high (Fig. 2A vs B, and Fig. 3C), similar to a previous CEST study on glycogen (van Zijl et al., 2007). With high labile proton concentration, linearity only holds for very small irradiation power and/or very short irradiation durations (Fig. 2A vs. B).

Although both are chemical exchange-based techniques, APEX shows positive contrast during ischemia, which is preferable to the negative contrast observed with APT, and better sensitivity than APT in many brain regions. More importantly, different spatial–temporal patterns were observed for these two approaches in our preliminary studies. In many animals, the lesion areas indicated by APEX maps were smaller (specifically, in the subcortical region) than those observed with APT (and ADC) maps. The APEX maps also showed greater temporal variation during the evolution of ischemia. Since the lesion volume and tissue outcome of the focal ischemia model are strongly dependent on the surgical procedure, the larger variation found with APEX maps suggests that the APEX signal may be more sensitive to physiological variations. Further studies will be performed to systematically compare the APEX maps with APT and ADC, as well as histology. The discrepancies between APEX and APT image contrast during focal ischemia suggest different underlying physiological sources. With APT, the CE agent is presumably derived from the amide protons of proteins and peptides, and the decrease of APT in the lesion area mainly reflects tissue acidosis since the concentration of proteins and peptides does not change significantly during initial hours of ischemia (Zhou et al., 2003). With APEX, the source of contrast is more complex because in addition to the proteins and peptides, free amino-acids also contribute to the signal, and these concentrations can vary significantly during the evolution of ischemia and may also be highly region-dependent. For example, it has been reported that for MCAO of 30 min to 4 h, there were strong regional and temporal dependent changes in the concentrations of glutamate, glutamine, and GABA. Specifically, in the lateral caudate-putamen and lower parietal cortex regions, the decrease of glutamate concentration was close to 50%, whereas the GABA concentration increased more than 100% at 4 h post MCAO (Haberg et al., 2001). Hence, the spatial–temporal mismatch between APT and APEX maps may be indicative of amino acid concentration change during ischemia and helps to understand disease evolution. Further study would be necessary to examine the physiological source of the APEX signal and its potential application in ischemia research.

Besides potential applications of APEX to pH-related research, such as ischemia and cortical spreading depression, the sensitivity of APEX to protein and amino acid concentration suggests that it may also be applicable to the study of many other diseases or physiological conditions.

Please cite this article as: Jin, T., et al., Magnetic resonance imaging of the Amine–Proton EXchange (APEX) dependent contrast, NeuroImage (2011), doi:10.1016/j.neuroimage.2011.08.014

For example, the concentration of amino acids, especially neurotransmitters like glutamate and GABA, may change significantly in pathological conditions such as neurodegenerative diseases, epilepsy or psychiatric disorders. As illustrated by proton spectroscopy studies, the concentration of glutamate, compared with total creatine level, decreases in the hippocampus of transgenic Alzheimer's disease (AD) mice (Marjanska et al., 2005), and can be used to distinguish the mild cognitive impairment with AD in human patients (Rupsingh et al., 2011). In addition, Zhou et al. (2008) showed that APT imaging can distinguish low- and high-grade glioma due to an increase of protein concentration with tumor grade. Due to its sensitivity in amino acid and protein concentrations, the APEX contrast may also be a potential biomarker in these applications.

Conclusion

The exchange between amine and water protons was measured with an SL technique that can be tuned to different CE rates to provide image contrast. Because of the similarity between CEST and off-resonance SL techniques, APEX contrast can also be obtained by a CEST approach using similar irradiation parameters. Compared to slow exchange applications, a higher SL irradiation power with shorter duration can optimize the APEX contrast, and the optimal irradiation time can be derived analytically with an SL model. APEX is sensitive to the concentration of proteins, peptides and amino acids, and is also sensitive to pH. With fast exchange rates and higher irradiation power, the specificity of CE contrast is reduced compared to slower exchange rates; thus, many different amine groups contribute the in vivo APEX signal, with weighting dependent on populations and exchange rates. In a rat MCAO model, APEX showed good sensitivity to the ischemic lesion and may provide complementary information compared to ADC and APT. APEX imaging may also provide a potential biomarker in pathological studies for conditions with variation in protein, peptide, or amino acid concentrations and/or pH.

Acknowledgments

We thank Kristy Hendrich for maintaining the 9.4 T system, Dr. Timothy Duong for providing a stroke animal protocol, and Dr. Kevin Hitchens for sharing a video of MCAO preparation. This work is supported by NIH grants EB008717, EB003324, EB003375, and NS44589.

References

Chen, J.H., Sambol, E.B., DeCarolis, P., O'Connor, R., Geha, R.C., Wu, Y.V., Singer, S., 2006. High-resolution MAS NMR spectroscopy detection of the spin magnetization exchange by cross-relaxation and chemical exchange in intact cell lines and human tissue specimens. Magnetic Resonance in Medicine 55, 1246–1256.

Haberg, A., Qu, H., Saether, O., Unsgard, G., Haraldseth, O., Sonnewald, U., 2001. Differences in neurotransmitter synthesis and intermediary metabolism between glutamatergic and GABAergic neurons during 4 hours of middle cerebral artery occlusion in the rat: the role of astrocytes in neuronal survival. Journal of Cerebral Blood Flow and Metabolism 21, 1451–1463.

Hindman, J.C., 1966. Proton resonance shift of water in the gas and liquid states. The Journal of Chemical Physics 44, 4582–4592.

Hua, J., Jones, C.K., Blakeley, J., Smith, S.A., van Zijl, P.C.M., Zhou, J.Y., 2007. Quantitative description of the asymmetry in magnetization transfer effects around the water resonance in the human brain. Magnetic Resonance in Medicine 58, 786–793.

Jin, T., Kim, S.-G., 2010. Change of the cerebrospinal fluid volume during brain activation investigated by T1ρ-weighted fMRI. Neuroimage 51, 1378–1383.

Jin, T., Autio, J., Obata, T., Kim, S.G., 2011. Spin-locking versus chemical exchange saturation transfer MRI for investigating chemical exchange process between water and labile metabolite protons. Magnetic Resonance in Medicine 65, 1448–1460.

Kim, M., Gillen, J., Landman, B.A., Zhou, J.Y., van Zijl, P.C.M., 2009. Water saturation shift referencing (WASSR) for chemical exchange saturation transfer (CEST) experiments. Magnetic Resonance in Medicine 61, 1441–1450.

Kiozumi, J., Yoshida, Y., Nakazawa, T., Ooneda, G., 1986. Experimental studies of ischemic brain edema: I: a new experimental model of cerebral embolism in rats in which recirculation can be introduced in the ischemic area. The Japanese Journal of Stroke 8, 1–8.

Liepinsh, E., Otting, G., 1996. Proton exchange rates from amino acid side chains — implications for image contrast. Magnetic Resonance in Medicine 35, 30–42.

Ling, W., Regatte, R.R., Navon, G., Jerschow, A., 2008. Assessment of glycosaminoglycan concentration in vivo by chemical exchange-dependent saturation transfer (gagCEST). Proceedings of the National Academy of Sciences of the United States of America 105, 2266–2270.

Marjanska, M., Curran, G.L., Wengenack, T.M., Henry, P.G., Bliss, R.L., Poduslo, J.F., Jack, C.R., Ugurbil, K., Garwood, M., 2005. Monitoring disease progression in transgenic mouse models of Alzheimer's disease with proton magnetic resonance spectroscopy. Proceedings of the National Academy of Sciences of the United States of America 102, 11906–11910.

McMahon, M.T., Gilad, A.A., Zhou, J.Y., Sun, P.Z., Bulte, J.W.M., van Zijl, P.C.M., 2006. Quantifying exchange rates in chemical exchange saturation transfer agents using the saturation time and saturation power dependencies of the magnetization transfer effect on the magnetic resonance imaging signal (QUEST and QUESP): pH calibration for poly-L-lysine and a starburst dendrimer. Magnetic Resonance in Medicine 55, 836–847.

McMahon, M.T., Gilad, A.A., DeLiso, M.A., Cromer Berman, S.M., Bulte, J.W.M., van Zijl, P.C.M., 2008. New "multicolor" polypeptide diamagnetic chemical exchange saturation transfer (DIACEST) contrast agents for MRI. Magnetic Resonance in Medicine 60, 803–812.

Mougin, O.E., Coxon, R.C., Pitiot, A., Gowland, P.A., 2010. Magnetization transfer phenomenon in the human brain at 7 T. NeuroImage 49, 272–281.

Narvainen, J., Hubbard, P.L., Kauppinen, R.A., Morris, G.A., 2010. Z-spectroscopy with alternating-phase irradiation. Journal of Magnetic Resonance 207, 242–250.

Rupsingh, R., Borrie, M., Smith, M., Wells, J.L., Bartha, R., 2011. Reduced hippocampal glutamate in Alzheimer disease. Neurobiology of Aging 32, 802–810.

Santyr, G.E., Fairbanks, E.J., Kelcz, F., Sorenson, J.A., 1994. Off-resonance spin locking for Mr-imaging. Magnetic Resonance in Medicine 32, 43–51.

Singh, A., Cai, K., Haris, M., Greenberg, J.H., Hariharan, H., Reddy, R., 2011. Dependence of CEST effect from amine protons of glutamate on pH. Proceedings of 19th ISMRM, Montreal, Canada, p. 713.

Sun, P.Z., van Zijl, P.C.M., Zhou, J.Y., 2005. Optimization of the irradiation power in chemical exchange dependent saturation transfer experiments. Journal of Magnetic Resonance 175, 193–200.

Sun, P.Z., Zhou, J.Y., Huang, J., van Zijl, P., 2007. Simplified quantitative description of amide proton transfer (APT) imaging during acute ischemia. Magnetic Resonance in Medicine 57, 405–410.

Sun, P.Z., Benner, T., Kumar, A., Sorensen, A.G., 2008. Investigation of optimizing and translating pH-sensitive pulsed-chemical exchange saturation transfer (CEST) imaging to a 3T clinical scanner. Magnetic Resonance in Medicine 60, 834–841.

Trott, O., Palmer, A.G., 2002. R-1 rho relaxation outside of the fast-exchange limit. Journal of Magnetic Resonance 154, 157–160.

van Zijl, P.C.M., Yadav, N.N., 2011. Chemical exchange saturation transfer (CEST): what is in a name and what isn't? Magnetic Resonance in Medicine 65, 927–948.

van Zijl, P.C.M., Jones, C.K., Ren, J., Malloy, C.R., Sherry, A.D., 2007. MRI detection of glycogen in vivo by using chemical exchange saturation transfer imaging (glycoCEST). Proceedings of the National Academy of Sciences of the United States of America 104, 4359–4364.

Ward, K.M., Aletras, A.H., Balaban, R.S., 2000. A new class of contrast agents for MRI based on proton chemical exchange dependent saturation transfer (CEST). Journal of Magnetic Resonance 143, 79–87.

Zhou, J.Y., van Zijl, P.C.M., 2006. Chemical exchange saturation transfer imaging and spectroscopy. Progress in Nuclear Magnetic Resonance Spectroscopy 48, 109–136.

Zhou, J.Y., Payen, J.F., Wilson, D.A., Traystman, R.J., van Zijl, P.C.M., 2003. Using the amide proton signals of intracellular proteins and peptides to detect pH effects in MRI. Nature Medicine 9, 1085–1090.

Zhou, J.Y., Wilson, D.A., Sun, P.Z., Klaus, J.A., van Zijl, P.C.M., 2004. Quantitative description of proton exchange processes between water and endogenous and exogenous agents for WEX, CEST, and APT experiments. Magnetic Resonance in Medicine 51, 945–952.

Zhou, J.Y., Blakeley, J.O., Hua, J., Kim, M., Laterra, J., Pomper, M.G., van Zijl, P.C.M., 2008. Practical data acquisition method for human brain tumor amide proton transfer (APT) imaging. Magnetic Resonance in Medicine 60, 842–849.

Please cite this article as: Jin, T., et al., Magnetic resonance imaging of the Amine–Proton EXchange (APEX) dependent contrast, NeuroImage (2011), doi:10.1016/j.neuroimage.2011.08.014